

---

# A Practical Layer-Parallel Training Algorithm for Residual Networks

---

Qi Sun<sup>\*1</sup> Hexin Dong<sup>\*1</sup> Zewei Chen<sup>\*2</sup> Weizhen Dian<sup>1</sup> Jiacheng Sun<sup>2</sup> Yitong Sun<sup>2</sup> Zhenguo Li<sup>2</sup> Bin Dong<sup>1</sup>

## Abstract

Gradient-based algorithms for training ResNets typically require a forward pass of the input data, followed by back-propagating the objective gradient to update parameters, which are time-consuming for deep ResNets. To break the dependencies between modules in both the forward and backward modes, auxiliary-variable methods such as the penalty and augmented Lagrangian (AL) approaches have attracted much interest lately due to their ability to exploit layer-wise parallelism. However, we observe that large communication overhead and lacking data augmentation are two key challenges of these methods, which may lead to low speedup ratio and accuracy drop across multiple compute devices. Inspired by the optimal control formulation of ResNets, we propose a novel serial-parallel hybrid training strategy to enable the use of data augmentation, together with downsampling filters to reduce the communication cost. The proposed strategy first trains the network parameters by solving a succession of independent sub-problems in parallel and then corrects the network parameters through a full serial forward-backward propagation of data. Such a strategy can be applied to most of the existing layer-parallel training methods using auxiliary variables. As an example, we validate the proposed strategy using penalty and AL methods on ResNet and WideResNet across MNIST, CIFAR-10 and CIFAR-100 datasets, achieving significant speedup over the traditional layer-serial training methods while maintaining comparable accuracy.

## 1. Introduction

Deep neural networks with millions of trainable parameters have become indispensable tools for machine learning applications involving large datasets (LeCun et al., 2015). For the

solution of such large-scale optimization problems, gradient-based algorithms are often employed, which requires a forward pass of the input data, followed by the backpropagation (Rumelhart et al., 1985) of objective gradients to update parameters in each iteration step. However, even with the use of modern Graphical Processing Units (GPUs), the overall training process still remains time-consuming. As such, various parallelization techniques including, but not limited to data-parallelism (Iandola et al., 2016), model-parallelism (Dean et al., 2012), and a combination of both (Paine et al., 2013; Harlap et al., 2018) have been proposed to reduce the training runtimes. Unfortunately, none of the above methods could tackle the scalability barrier created by the intrinsically serial propagation of data within the network (Günther et al., 2020), preventing us from updating layers in parallel and fully leveraging the computing resources.

One way of achieving speed-up over the traditional methods is to apply synthetic gradients to build decoupled neural interfaces (Jaderberg et al., 2017), where the objective gradients are approximated by additional neural networks so that each layer can be locally updated without performing the full serial backpropagation. However, it fails in training deep convolutional networks since the construction of synthetic loss function has little relation to the target objective function (Miyato et al., 2017). Another related work is proposed in (Huo et al., 2018), where the authors use stale gradients to remove the backward locking. Such a method, though effective, requires a full serial forward pass before executing the decoupled parallel backpropagation, thereby the upper bound of the resulting speed-up is very limited according to Amdahl’s law (Gustafson, 1988).

To exploit layer-wise parallelism in both the forward and backward modes, several algorithms were proposed recently by introducing auxiliary variables associated with the decoupled neural interfaces, *e.g.*, the quadratic penalty method (Carreira-Perpinan and Wang, 2014; Zeng et al., 2018; Choromanska et al., 2018), the augmented Lagrangian (AL) method (Taylor et al., 2016; Zeng et al., 2019; Marra et al., 2020) and the proximal method (Li et al., 2020) for training fully-connected networks, which can achieve speed-up over the traditional layer-serial training method on a single Central Processing Unit (CPU) (Li et al., 2020). However, as shown in (Gotmare et al., 2018) and commented in (Huo et al., 2018), the performances of most of these methods are

---

<sup>\*</sup>Equal contribution <sup>1</sup>Peking University <sup>2</sup>Huawei Noah’s Ark Lab. Correspondence to: Qi Sun <qsun2019@pku.edu.cn>, Bin Dong <dongbin@math.pku.edu.cn>.

much worse than the backpropagation algorithm for deep convolutional neural networks. In other recent approaches (Günther et al., 2020; Parpas and Muir, 2019; Kirby et al., 2020), based on the similarity of ResNets training to the optimal control of nonlinear systems (E, 2017), parareal method for solving differential equations is employed to replace the forward pass and backpropagation with iterative multigrid schemes respectively. Since the feature maps need to be recorded at each module and then used in a subsequent process to solve the adjoint equation (Tröltzsch, 2010), experiments were conducted on simple ResNets across small datasets, rather than state-of-the-art ResNets across larger datasets. So far, to the best of our knowledge, it is uncertain that whether these layer-parallel training strategies can be effectively and efficiently applied to modern deep networks across real-world datasets.

In this work, we observe that there are two key issues that prevent us from attaining good performance in practical scenarios. The accuracy drop of trained model is mainly due to the lack of data augmentation, which is hard to implement at the presence of auxiliary variables. Furthermore, data communication is another potential issue that may hamper the speed-up ratio, which was not adequately addressed in previous studies since most implementations were conducted on CPUs. Based on these observations and inspired by optimal control formulation of training ResNets, we propose a novel serial-parallel hybrid (SPH) training strategy that alternates between the traditional layer-serial training with data augmentation and the layer-parallel training in a reduced parameter space. Here, layer-serial training allows the use of data augmentation while layer-parallel training in a reduced parameter space is achieved by downsampling (DS) of the auxiliary variables to alleviate the communication burden.

The contribution of this work is threefold:

- (1) We observe that large communication overhead and the lack of data augmentation are two key challenges for auxiliary-variable methods, which may lead to accuracy drop and low speedup ratio across multiple computing devices.
- (2) A novel SPH strategy is proposed to enable the use of data augmentation during training, together with the employment of downsampling filters to reduce the communication cost.
- (3) We validate our methods on ResNet and WideResNet across MNIST, CIFAR-10, and CIFAR-100 datasets, achieving significant speed-up over the traditional layer-serial training methods while maintaining comparable accuracy.

The rest of this paper is organized as follows. Section 2 is devoted to recalling the backpropagation algorithm and locking effects during training, followed by the layer-parallel

training of ResNets from a dynamical systems viewpoint (see Figure 1). The downsampling filters and SPH strategy are proposed in Section 3 to handle the issues of data communication and data augmentation. Experimental results are presented in Section 4 to validate our theoretical findings.

## 2. Preliminaries

### 2.1. Layer-Serial Training

Based on the concept of modified equations (E, 2017) or the variational analysis using  $\Gamma$ -convergence (Thorpe and van Gennip, 2018), training of the ResNets from scratch (He et al., 2016a;b) (see Appendix A for notation description)

$$\arg \min_{\{W_\ell\}_{\ell=0}^{L-1}} \left\{ \varphi(X_L) \mid X_0 = S(y), X_{\ell+1} = X_\ell + F(X_\ell, W_\ell) \right\} \quad (1)$$

can be interpreted as the discretization of a terminal control problem governed by the so-called neural ODE (Chen et al., 2018)

$$\arg \min_{w_t} \left\{ \varphi(x_1) \mid x_0 = S(y), dx_t = f(x_t, w_t) dt \right\}. \quad (2)$$

For the ease of comparison, we refer, respectively, to (1) and (2) as the layer-serial and time-serial training method, and the same is said for their variants in the following sections.

Moreover, given a learning rate  $\eta > 0$ , the continuous-time counterpart of the backpropagation algorithm (Hecht-Nielsen, 1992) for solving (1), *i.e.*, for  $0 \leq \ell \leq L - 1$ ,

$$W_\ell \leftarrow W_\ell - \eta \frac{\partial \varphi(X_L)}{\partial X_{\ell+1}} \frac{\partial F(X_\ell, W_\ell)}{\partial W_\ell}, \quad (3)$$

is handled by the adjoint and control equations for finding the extremal of (2) (Li et al., 2017), that is,

$$dp_t = -p_t \frac{\partial f(x_t, w_t)}{\partial x} dt, \quad p_1 = \frac{\partial \varphi(x_1)}{\partial x}, \quad (4)$$

$$w_t \leftarrow w_t - \eta p_t \frac{\partial f(x_t, w_t)}{\partial w}, \quad 0 \leq t \leq 1, \quad (5)$$

where  $p_t$  is the adjoint variable that captures the objective changes with respect to hidden neurons (see Appendix A).

As a result, the *locking* effects (Jaderberg et al., 2017) for training feedforward neural networks, *i.e.*,

- (i) forward locking: no module can process its incoming data before the previous node in the directed forward network have executed;
- (ii) backward locking: no module can capture the objective changes with respect to its activation layer before the previous node in the backward network have executed;
- (iii) update locking: no module parameters can be updated before all the dependent nodes have executed in both the forward and backward modes;

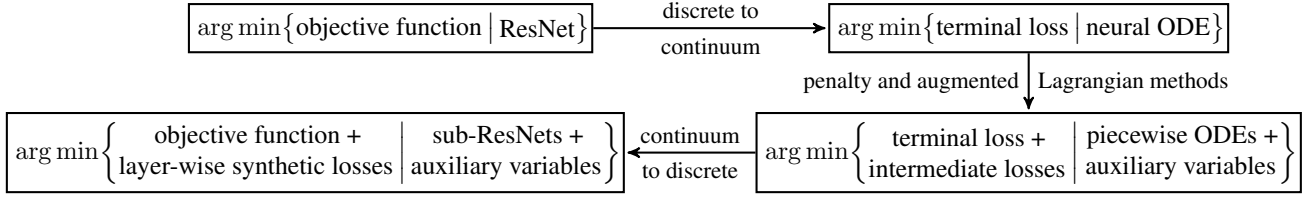


Figure 1. A diagram describing the construction of parallel training algorithm from the dynamical systems view.

can be recast as the necessity of solving both the neural ODE in (2) and a backward-in-time adjoint equation (4) in order to perform the control updates (5).

This connection not only brings us a dynamical system view of the locking effects but also provides a way to consistently discretize the iterative system (4) and (5) for solving the continuous-time optimization problem (2). Although recent hardware developments have gradually increased the capability of data-parallelism (Iandola et al., 2016), model-parallelism (Dean et al., 2012), and a combination of both (Paine et al., 2013; Harlap et al., 2018) for training large-scale neural networks, none of them could overcome the scalability barrier caused by the serial forward-backward propagation of data through the network (Günther et al., 2020). As such, breaking the locking issues, or, equivalently, parallelizing the iterative system for solving (2) is another promising approach to speed up the training.

## 2.2. Layer-Parallel Training

The similarity of training ResNets to the terminal control of ODEs motivates us to use the parallel-in-time methods (Maday and Turinici, 2002; Carraro et al., 2015) to achieve concurrency across all the network modules (see Figure 1).

### 2.2.1. FORWARD PASS WITH AUXILIARY VARIABLES

That is, to employ  $K \in \mathbb{N}_+$  independent processors for the solution of neural ODE in (2), we introduce a partition of  $[0, 1]$  into several disjoint intervals as shown in Figure 2

$$0 = s_0 < \dots < s_k < s_{k+1} < \dots < s_K = 1.$$

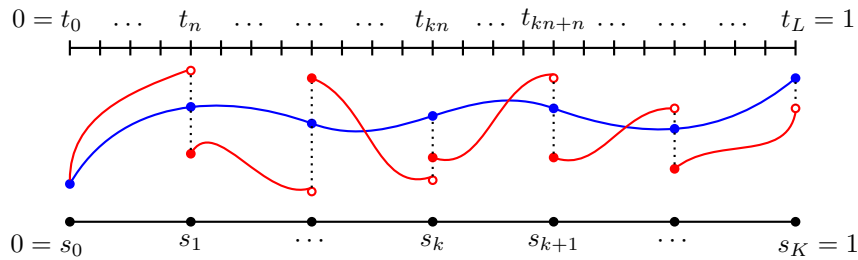


Figure 2. Contrary to the trajectory of neural ODE (blue line), introducing auxiliary variables (solid red dots) for each local sub-problem (red lines) enables a time-parallel computation of the state, adjoint, and control variables. Note that to approximately recover the serial approach, violation of equality constraints (mismatch between solid and hollow red dots) should be penalized in the objective function.

Now we are ready to define the piecewise states  $\{x_t^k\}_{k=0}^{K-1}$  such that the underlying dynamic evolves according to

$$x_{s_k^+}^k = \lambda_k, \quad dx_t^k = f(x_t^k, w_t^k)dt \text{ on } (s_k, s_{k+1}], \quad (6)$$

*i.e.*, the continuous-time forward pass that originates from auxiliary variable  $\lambda_k$  and with control variable  $w_t^k$ . Here,  $x_{s_k^+}^k$  and  $x_{s_k^-}^k$  refer to the right and left limits of the possibly discontinuous function  $x_t^k$  at the interface  $t = s_k$ .

Clearly, the state variable of problem (2) satisfies  $x_t = x_t^k$  for any  $t \in [s_k, s_{k+1}]$  and  $0 \leq k < K - 1$  if and only if

$$w_t^k = w_t|_{(s_k, s_{k+1})} \quad \text{and} \quad \lambda_k = x_{s_k^+}^k,$$

or, equivalently,  $\lambda_k = x_{s_k^-}^{k-1}$  with  $x_{s_0^-}^{-1} = x_0$  to replace the second condition. As a result, the optimization problem (2) can be reformulated as

$$\arg \min_{\{w_t^k, \lambda_k\}_{k=0}^{K-1}} \left\{ \varphi(x_{s_K^-}^{K-1}) \mid x_{s_k^-}^{k-1} = \lambda_k \text{ and (6)} \right\} \quad (7)$$

which offers the possibility of parallelizing the evolution of dynamical system (6) by relaxing the other constraint, *e.g.*, Figure 2 with external auxiliary variables.

### 2.2.2. AUGMENTED LAGRANGIAN METHOD

Formula (7) implies that the exact connection between adjacent intervals can be loosened by incorporating external auxiliary variables, which inspires us to relax the equality constraints and add penalties to the objective function, *i.e.*,

$$\arg \min_{\{w_t^k, \lambda_k\}_{k=0}^{K-1}} \left\{ \varphi(x_{s_K^-}^{K-1}) + \beta \sum_{k=0}^{K-1} \psi(\lambda_k, x_{s_k^-}^{k-1}) \mid (6) \right\} \quad (8)$$

**Algorithm 1:** Layer-parallel Training Algorithm (Non-intrusive Implementation Details)

```

// Initialization (see Appendix D for more details).
// Training Procedure.
for j ← 1 to J (number of training epochs) do
  foreach mini-batch input data do
    // decoupled parallel forward-backward propagation on multiple GPUs
    parfor k ← 0 to K - 1 do
      // forward pass with auxiliary variable loading from CPU
      for m ← 0 to n - 1 do
        |  $X_{kn}^k = \lambda_k, X_{kn+m+1}^k = X_{kn+m}^k + F(X_{kn+m}^k, W_{kn+m}^k)$ 
      // backpropagation with synthetic and objective loss functions
      for m ← n to 0 do
        | if  $k \neq K - 1$  then
        | |  $W_{kn+m}^k \leftarrow W_{kn+m}^k - \eta_w \left( \beta \frac{\partial \psi(X_{kn+n}^k, \lambda_{k+1})}{\partial W_{kn+m}^k} + \kappa_{k+1} \frac{\partial X_{kn+n}^k}{\partial W_{kn+m}^k} \right)$ 
        | | else
        | |  $W_{kn+m}^k \leftarrow W_{kn+m}^k - \eta_w \frac{\partial \varphi(X_{kn+n}^k)}{\partial W_{kn+m}^k}$ 
      // communication across GPUs and data transmission from GPUs to CPU
      for k ← 1 to K - 1 do
        // correction of auxiliary variable
        | if  $k \neq K - 1$  then
        | |  $\lambda_k \leftarrow \lambda_k - \eta_\lambda \left( \beta \frac{\partial \psi(\lambda_k, X_{kn}^{k-1})}{\partial \lambda_k} + \beta \frac{\partial \psi(X_{kn+n}^k, \lambda_{k+1})}{\partial X_{kn}^k} + \kappa_{k+1} \frac{\partial X_{kn+n}^k}{\partial X_{kn}^k} - \kappa_k \right)$ 
        | | else
        | |  $\lambda_k \leftarrow \lambda_k - \eta_\lambda \left( \frac{\partial \varphi(X_{kn+n}^k)}{\partial X_{kn}^k} - \kappa_k \right)$ 
        // update of Lagrangian multiplier
         $\kappa_k \leftarrow \kappa_k - \frac{\eta_\kappa}{2\beta} (\lambda_k - X_{kn}^{k-1})$  // designed for quadratic penalty function

```

where  $\beta > 0$  is a scalar constant and  $\psi(\lambda, x) = \|\lambda - x\|_{\ell_2}^2$  the quadratic penalty function. Such a method has been extensively used due to its simplicity and intuitive appeal (Taylor et al., 2016; Choromanska et al., 2018; Gotmare et al., 2018), however, it suffers from ill-conditioning when the penalty coefficient is large (Nocedal and Wright, 2006).

To make the approximate solution of (8) nearly satisfy the layer-serial approach (2) even for moderate values of  $\beta$ , we consider the augmented Lagrangian of problem (7)

$$\mathcal{L}(x_t^k, p_t^k, w_t^k, \lambda_k, \kappa_k) = \varphi(x_{s_k}^{K-1}) + \sum_{k=0}^{K-1} \left( \beta \psi(\lambda_k, x_{s_k}^{k-1}) + \int_{s_k}^{s_{k+1}} p_t^k (f(x_t^k, w_t^k) - \dot{x}_t^k) dt - \kappa_k (\lambda_k - x_{s_k}^{k-1}) \right)$$

where  $\kappa_k$  denotes an explicit Lagrange multiplier. Notably, by forcing  $\kappa_k \equiv 0$  for any  $0 \leq k \leq K - 1$ , the augmented Lagrangian method degenerates the penalty approach.

To clarify the differences between layer-parallel training of fully-connected networks (Zeng et al., 2019) and ResNets,

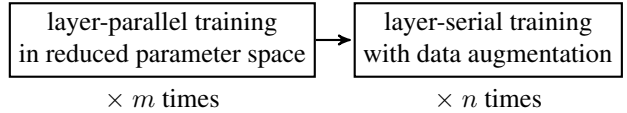


Figure 3. A diagram describes the serial-parallel hybrid strategy.

we refer the readers to Figure 1 for technical details. Specifically, the iterative system for solving the relaxed optimization problems is provided in Appendix B, which results in a non-intrusive layer-parallel training algorithm after employing the consistent discretization schemes discussed in Appendix A. Implementation details are summarized in Algorithm 1, which includes both the AL and penalty (achieved by forcing  $\kappa_k \equiv 0$  during training) methods.

### 3. Method

We note that the external auxiliary variables increases concurrency across all the network modules but incurs additional memory and communication overheads, which may limit the performance for the exposed parallelism especially

in the setting of fine partitioned models with data augmentation. Therefore, a novel method with serial-parallel hybrid training strategy and downsampling strategy is proposed to handle these issues (see Figure 3 for the schematic of the proposed strategy). We also note that our strategy is effective on any layer-parallel training algorithm that introduces auxiliary variables.

### 3.1. Downsampling for Data Communication

For each iteration of Algorithm 1, the computational time associated with the layer-serial ( $K = 1$ ) and layer-parallel ( $K > 1$ ) training approaches can be summarized as follows:

	layer-serial	layer-parallel
forward pass	$t_f$	$\frac{1}{K}t_f$
backpropagation	$t_b$	$\frac{1}{K}t_b + t_\psi$
communication	$t_d$	$t_\lambda + t_\kappa$

where  $t_f$  ( $t_b$ ) denotes the time cost of forward pass (back-propagation) using the layer-serial training method,  $t_d$  the time cost on data loader,  $t_\psi$  the computation time of synthetic loss functions,  $t_\lambda + t_\kappa$  the evaluation and communication time of auxiliary variables. Clearly, the speedup ratio per epoch can be expressed as

$$\rho_K = \frac{\text{serial runtime}}{\text{parallel runtime}} = \frac{1}{\frac{1}{K} \frac{t_f + t_b}{t_f + t_b + t_d} + \frac{t_\psi + t_\lambda + t_\kappa}{t_f + t_b + t_d}} \quad (9)$$

where  $t_f$ ,  $t_b$ ,  $t_d$ ,  $t_\psi$ ,  $t_\lambda$  and  $t_\kappa$  are almost independent of the model partition number  $K$  during training.

Note that for realistic neural networks such as ResNets (He et al., 2016a;b), it is plausible to assume that  $t_f + t_b + t_d > t_\psi + t_\lambda + t_\kappa$ , which immediately shows speed-up over the traditional layer-serial training approach by choosing a sufficient large value of  $K$ . Notably, formula (9) also implies that the upper bound of speed-up ratio is given by

$$\rho_K < \frac{t_f + t_b + t_d}{t_\psi + t_\lambda + t_\kappa},$$

namely, the communication becomes the performance bottleneck as the model is partitioned more finely, which motivates us to reduce the data communication overhead in order to further accelerate the network training.

One way to achieve this is to design downsampling (DS) filters to attenuate the size of auxiliary variables. We can, for instance, take the example of penalty method (8). Instead of transferring the full-size auxiliary variables between CPU and GPU cores, we can operate with the downsampled data

$$\Lambda_k = \text{DS}(\lambda_k), \text{ or approximately, } \lambda_k \approx \text{US}(\Lambda_k)$$

to execute the forward pass (6) for  $0 \leq k \leq K - 1$

$$x_{s_k}^k = \text{US}(\Lambda_k), \quad dx_t^k = f(x_t^k, w_t^k) dt \text{ on } (s_k, s_{k+1}]. \quad (10)$$

For instance, by taking the Kronecker product with an all-ones matrix of size  $2 \times 2$  for each slice of the tensor  $\Lambda_k$ , we obtain the auxiliary variable  $\lambda_k$  for forward pass. section 4 will focus on this particular example and we leave the exploration of other downsampling tools as future work.

As such, the optimization problem is now defined in a reduced parameter space, that is,

$$\arg \min_{\{w_t^k, \Lambda_k\}_{k=0}^{K-1}} \left\{ \varphi(x_{s_K}^{K-1}) + \beta \sum_{k=0}^{K-1} \psi(\text{US}(\Lambda_k), x_{s_k}^{k-1}) \right\} \quad (10)$$

With a slight loss of accuracy, the memory and communication overheads can be significantly reduced compared with the original method (8). Moreover, the implementation is very straightforward, only requiring an additional upsampling layer before the execution of forward pass in Algorithm 1, while the backpropagation is automatically achieved through the standard auto-differentiation. Such a technique can also be easily extended to the augmented Lagrangian method (omitted here for simplicity).

### 3.2. Hybrid Training for Data Augmentation

Another key observation is that each training sample requires to introduce a group of corresponding auxiliary variables. These auxiliary variables need to be stored and recomputed during the iteration. When cooperating with the commonly used data augmentation (Tanner and Wong, 1987) which reduce overfitting by artificially increasing the number of samples in the training set, extra auxiliary variables need to introduce for each augmented sample. It would incur prohibitive memory requirements making great challenge to incorporate data augmentation. We believe that this is the key reason that previous methods' performance is far below the state-of-the-art.

To justify our argument, we shown some preliminary experimental results by using different ratios  $\rho_{\text{DA}}$  of data augmentation (*i.e.*, the number of synthetic images to the number of real images), Figure 4 shows the test accuracy of ResNet-110 for the classification task on CIFAR-10 dataset, where  $\rho_{\text{DA}} = \infty$  denotes the data augmentation containing random operations. It can be observed that, as  $\rho_{\text{DA}}$  is increased, the accuracy gap between the traditional layer-serial training method and the proposed layer-parallel training approach is tending to close. However, the memory requirements for storing all the synthetic training data blows up even for moderate values of  $\rho_{\text{DA}}$ , which is unaffordable in practical scenarios.

Unfortunately, most of the existing auxiliary-variable methods fail to address this issue, which often leads to a significant accuracy drop of the trained networks (Gotmare et al., 2018). To allow the use of data augmentation during training, we propose a novel serial-parallel hybrid (SPH)

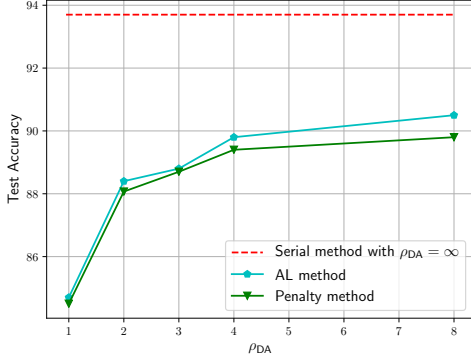


Figure 4. Test accuracy of trained model using data augmentation.

strategy that alternatives between the layer-serial and layer-parallel training modes as depicted in Figure 3. That is, the layer-parallel training method is performed  $m$  times without data augmentation, followed by  $n$  times execution of the layer-serial training method, which improves the network parameters through the employment of data augmentation.

As an immediate result, the speed-up ratio now gives

$$\rho_H = \frac{(m+n) \times t_s}{m \times t_p + n \times t_s} = \frac{1 + \gamma_H}{\frac{1}{\rho_K} + \gamma_H} \quad (11)$$

where  $\gamma_H = \frac{n}{m}$  indicates the hybrid ration,  $t_s = t_f + t_b + t_d$  and  $t_p = \frac{1}{K}(t_s + t_b) + t_\psi + t_\lambda + t_\kappa$  are runtime of the layer-serial and layer-parallel training methods per epoch. Although the serial portions in (11) hamper the speedup ratio, *i.e.*,  $\rho_H < \rho_K$ , enabling data augmentation can significantly increase the test accuracy as shown in Figure 4. Moreover, the constraint violations caused by downsampling, *i.e.*,  $US(\Lambda_k)$  is applied to match  $x_{s_k}^{k-1}$  in (3.1) instead of  $\lambda_k$ , can be adjusted through the layer-serial training procedure, which also works for applications without the use of data augmentation. Experimental results in section 4 validate our theoretical findings.

## 4. Experiments

To verify our method’s effectiveness, we conduct experiments on various settings, including different datasets, network architectures and tasks. Firstly, in Section 4.1 we verify our method with image classification on CIFAR-10 and CIFAR-100, respectively. We show that the proposed SPH and DS can effectively deal with the issues on data augmentation and communication, respectively. Moreover, the combination of DS and SPH (DS-SPH) achieves comparable performance with traditional serially training methods while maintaining a competitive speed-up ratio. Secondly, in Section 4.2 we conduct the experiment on image generation to show that our method is not limited to classification. As data augmentation is usually not considered in image generation, our method shows a significantly speed-up ratio

(SUR) with quite well generation performance. For simplicity, we use DS-SPH-P and DS-SPH-AL to represent penalty based DS-SPH method and AL-based DS-SPH method.

All of our experiments are implemented in Pytorch 1.4. Our model is split into  $K$  stages, distributed on  $K$  GPUs (Tesla-V100). The parallel methods are implemented based on the Pytorch multiprocessing library with NCCL backends.

### 4.1. Images Classification

In this section, we verify our methods for classification tasks on CIFAR-10 and CIFAR-100.

**Implementation Details:** For CIFAR-10, the serial model is implemented based on **ResNet-110**. For penalty and AL methods, the networks are divided into **two or three stages**. Empirically, we set the initial penalty coefficient  $\beta = 100$ . For all experiments, we use SGD optimizer with initial learning rate 0.1. We train our models for 200 epochs and decay the learning rate (lr) by 0.1 for every 50 epochs. For CIFAR-100, the serial model is implemented based on **WideResNet** with 40 layers and widen factor 10 (WideResNet-40-10). We set the penalty coefficient  $\beta = 10$  as we empirically found it works better for WideResNet. For all experiments on CIFAR-100, we use SGD optimizer with initial learning rate 0.1. We train our models for 200 epochs and decay lr according to cosine-lr schedule. Results of CIFAR-10 and CIFAR-100 are summarized in Table 1 and Table 2.

**Benefit of Serial-Parallel-Hybrid Strategy.** The performance of vanilla penalty and AL methods are much worse than the traditional serial training with data augmentation (with approximately 8% accuracy drop from 93.7% to 85.7% for AL  $K = 2$ , see Table 1). This is mainly caused by lacking data augmentation (DA), as analyzed in the last section. But with our 1:4 hybrid ratio training strategy, parallel training with 80% epochs before serial training for the other 20%, SPH-AL  $K = 2$  gets test accuracy 91.8%, reducing the gap to serial training with DA from 8% to 2%. This remarkable improvement only causes a slight drop in the speed-up ratio, which is acceptable in practice. Besides, the AL methods are slightly better than the penalty method in terms of test accuracy while at the cost of higher memory load and lower speed-up ratio.

**Benefit of Down-Sampling Strategy.** Apart from the DA problem, another critical problem that limits the penalty and AL parallel methods’ efficiency is the storage and CPU-GPU communication of auxiliary variables. Due to the large size of auxiliary variables, these variables cannot be stored directly in GPU memory. We have to save them in the CPU memory and load them to GPU in the training process. The frequent CPU-GPU communication causes a huge communication overhead. Comparing the results of penalty

Table 1. Memory, test accuracy and SURs of ResNet-110 on CIFAR-10, where  $K = 2, 3$  and hybrid ratio  $\gamma_H = 1 : 4$ .

Method	Memory (GB)	Test Acc.	SURs	Method	Memory (GB)	Test Acc.	SURs
Serial w/o DA	-	86.4	-	Serial with DA	-	93.7	-
Penalty ( $K = 2$ )	1.53	85.0	1.41	AL ( $K = 2$ )	3.05	85.7	1.36
Penalty ( $K = 3$ )	4.58	84.5	1.56	AL ( $K = 3$ )	9.12	85.2	1.49
DS-P ( $K = 2$ )	0.38	84.2	1.53	DS-AL ( $K = 2$ )	0.57	84.1	1.42
DS-P ( $K = 3$ )	1.44	83.7	1.69	DS-AL ( $K = 3$ )	2.29	83.7	1.58
SPH-P ( $K = 2$ )	1.53	91.8	1.30	SPH-AL ( $K = 2$ )	3.05	91.8	1.27
SPH-P ( $K = 3$ )	4.58	91.3	1.40	SPH-AL ( $K = 3$ )	9.12	91.4	1.35
DS-SPH-P ( $K = 2$ )	0.38	91.8	1.38	DS-SPH-AL ( $K = 2$ )	0.57	91.6	1.31
DS-SPH-P ( $K = 3$ )	1.44	91.8	1.48	DS-SPH-AL ( $K = 3$ )	2.29	91.5	1.41

Table 2. Memory, test accuracy and SURs of WideResNet on CIFAR-100, where  $K = 3$  and hybrid ratio  $\gamma_H = 1 : 4$ .

Method	Memory (GB)	Test Acc.	SURs	Method	Memory (GB)	Test Acc.	SURs
Serial w/o DA	-	66.53	-	Serial with DA	-	80.71	-
Penalty	45.77	64.91	1.89	AL	91.55	64.80	1.67
DS-P	11.44	61.06	2.19	DS-AL	22.89	60.84	1.92
SPH-P	45.77	75.25	1.52	SPH-AL	91.55	76.25	1.42
DS-SPH-P	11.44	76.23	1.76	DS-SPH-AL	22.89	76.84	1.62

and downsampling with the penalty (DS-P), downsampling the feature maps hurts the performance less than 1% (decrease from 84.5% to 83.7% with  $K = 3$  in Table 1) but significantly reduces the memory cost at least three times ( $4.58/1.44 \approx 3.18$ ) and increases the speed-up ratio 1.56 to 1.69. Interestingly, although the down-sampling strategy alone decreases the test accuracy slightly, it improves the performance by 0.5% when combined with SPH.

**More Complicate Model and Dataset.** We have shown that our method works well on CIFAR-10 with ResNet. For more complicated datasets and models, our methods still work well. We also verify our method on CIFAR-100 with WideResNet. The feature map of WideResNet is much larger than ResNet. Specifically, the feature map of WideResNet-40-10 is ten times larger than that of ResNet. Therefore, we need to introduce many auxiliary variables for WideResNet, which makes the parallelization even more challenging. From Table 2 we see that our method also shows its superiority in training WideResNet. The performance gap between the serial training with data augmentation and vanilla parallel training, which is penalty and AL, is about 15%, much larger than that of CIFAR-10 with ResNet. Our method decreases this gap to 4.48% and 3.7% for penalty and AL, respectively. Furthermore, the speed-up ratio is larger than that in ResNet, say 1.76 compares to 1.48 for DS-SPH-P and 1.62 compares to 1.41 for DS-SPH-AL. It is because a large number of auxiliary variables naturally lead to larger memory cost and communication overhead. Our DS strategy reduces much cost in them and exhibits a more speed-up ratio.

**Accuracy-Speed Trade-off.** In this part, we study the accuracy-speed trade-off from two aspects, the number of stages  $K$  and the hybrid ratio. Results of  $K = 2$  and  $K = 3$

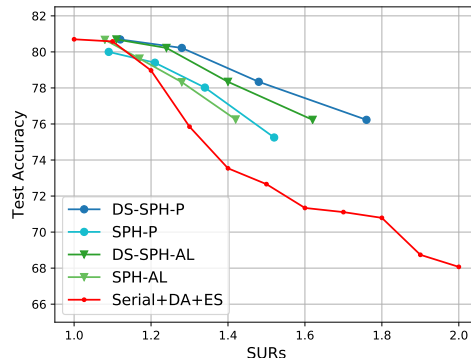


Figure 5. Accuracy-speed trade-off for different methods. The red-dot line is drawn by early stopping (ES) the serial training at epochs corresponding to the speed-up ratio. The DS-SPH methods dominate other methods.

for different methods on CIFAR-10 are shown in Table 1. The more stages we divide the model, the more auxiliary variables we need to introduce and the more computing resource we need. Therefore, in general, the memory cost and speed-up ratio grow as  $K$  grows large. However, more auxiliary variables also introduce more constraints to the optimization problem making it more difficult to solve. Thus, more stages often leads to a performance drop, while such drop may be negligible. These results are observed in Table 1 for all methods. More specifically, when increasing  $K$  from 2 to 3 DS-SPH-AL's performance drops from 91.6% to 91.5% with the speed-up ratio increasing from 1.31 to 1.41. There is no performance difference up to the first decimal when increasing  $K$  from 2 to 3 for DS-SPH-P.

The other factor which affects the accuracy-speed trade-off is the hybrid ratio  $\gamma_H$ . In Table 3 and Table 4, we show the results of different  $\gamma_H$  on CIFAR-10 and CIFAR-100,

Table 3. For ResNet-110 on CIFAR-10,  $\gamma_H$ , SURs, test accuracy of SPH and DS-SPH using penalty and AL methods.

$\gamma_H$	Methods	Penalty		AL	
		SURs	Test Acc.	SURs	Test Acc.
1:4	SPH	1.40	91.25	1.35	91.38
2:3	SPH	1.27	92.36	1.24	92.64
3:2	SPH	1.16	92.85	1.14	93.13
4:1	SPH	1.07	93.18	1.07	93.75
1:4	DS-SPH	1.48	91.75	1.41	91.54
2:3	DS-SPH	1.32	92.79	1.28	92.58
3:2	DS-SPH	1.19	93.58	1.17	93.11
4:1	DS-SPH	1.08	93.62	1.08	93.66
-	Serial+DA	-	93.70		

Table 4. For WideResNet on CIFAR-100,  $\gamma_H$ , SURs, test accuracy of SPH and DS-SPH using penalty and AL methods.

$\gamma_H$	Methods	Penalty		AL	
		SURs	Test Acc.	SURs	Test Acc.
1:4	SPH	1.52	75.25	1.42	76.25
2:3	SPH	1.34	78.02	1.28	78.32
3:2	SPH	1.21	79.40	1.17	79.63
4:1	SPH	1.09	80.00	1.08	80.67
1:4	DS-SPH	1.76	76.23	1.62	76.84
2:3	DS-SPH	1.48	78.34	1.40	78.08
3:2	DS-SPH	1.28	80.22	1.24	79.97
4:1	DS-SPH	1.12	80.69	1.11	80.37
-	Serial+DA	-	80.70		

respectively. As  $\gamma_H$  increases, the speed-up ratio decreases accordingly, but the performances become closer to the serial training results. To be more specific, take DS-SPH-P as an example, when  $\gamma_H = 1:4$ , the test accuracy is 91.25% with a speed-up ratio of 1.40. As increasing  $\gamma_H$  to 4:1, the test accuracy approach to 93.62%, which is very close to the serial training result of 93.70%. In Figure 5, we compare this trade-off of CIFAR-100 between different methods. Our DS-SPH method consistently outperforms other methods.

## 4.2. Image Generation

This section shows the experimental results on the image generation task to demonstrate that our method is not limited to image classification.

**Implementation Details:** A VAE (Kingma and Welling, 2013) model contains a pair of encoder and decoder. The serial model is implemented based on ResNet-VAE whose encoder is ResNet-110. The encoder for penalty method and AL method is divided to **three stages** and the initial penalty coefficient  $\beta$  is set as 10. We use Adam as an optimizer for all networks, and the initial learning rate is set as 0.01. To evaluate the generated image, we use the reconstructing MSE loss between reconstructed images and original images on the test set.

The results are shown in Table 5. As data augmentation

Table 5. Test loss and SURs based on above two methods with  $K=3$  and hybrid ratio  $\gamma_H = 1:4$  on MNIST Generation.

METHOD	TEST LOSS	SUR
SERIAL MODEL	0.126	-
PENALTY	0.149	2.33
AL	0.129	2.18
DS-P	0.160	2.41
DS-AL	0.137	2.25
DS-SPH-P	0.127	1.88
DS-SPH-AL	0.128	1.80



Figure 6. Results for reconstruction images in test set. **Line-1:** Original images; **Line-2:** Reconstruction from serial method; **Line-3:** Reconstruction from DS-SPH using penalty method; **Line-4:** Reconstruction images from DS-SPH using AL method.

is usually not used in the training of VAE, we omit the experiments with only SPH. As the results show, the vanilla penalty and AL, in general, can achieve acceptable performance on VAE, since data augmentation is not essential. However, they still suffer from enormous memory cost and CPU-GPU communication overhead. DS strategy reduces those costs significantly with a slight drop in performance. The reconstruction loss reduces from 0.149 to 0.160 for DS-P and from 0.129 to 0.137 for DS-AL. Combining with SPH, the performance drop caused by DS is almost eliminated. This result shows that SPH plays a more significant role than merely providing data augmentation. It also helps eliminate the gap between the real feature map and the auxiliary feature map and get better results, in Figure 6 we show the reconstructed images sampled from the test set to examine their visual qualities. From the figure, we see that our methods indeed reconstruct high-quality images.

## 5. Conclusion

In this paper, we observed that the key issues that hampered the practicality of layer-parallel training were data augmentation and communication. We then proposed a novel hybrid training strategy combined with downsampling to resolve the aforementioned issues, and demonstrated the effectiveness of the proposed method on training large residual networks on CIFAR-10 and CIFAR-100. Potential future directions include investigation on the proposed method with more heavy duty deep residual networks, larger number of stages, exploring other choices of downsampling operators, other layer-parallel training algorithms, etc.



## References

- T. Carraro, M. Geiger, S. Rorkel, and R. Rannacher. *Multiple Shooting and Time Domain Decomposition Methods*. Springer, 2015.
- M. Carreira-Perpinan and W. Wang. Distributed optimization of deeply nested systems. In *Artificial Intelligence and Statistics*, pages 10–19. PMLR, 2014.
- R. Chen, Y. Rubanova, J. Bettencourt, and D. Duvenaud. Neural ordinary differential equations. In *Advances in Neural Information Processing Systems*, 2018.
- A. Choromanska, B. Cowen, S. Kumaravel, R. Luss, M. Rigotti, I. Rish, B. Kingsbury, P. DiAchille, V. Gurev, R. Tejwani, et al. Beyond backprop: Online alternating minimization with auxiliary variables. *arXiv preprint arXiv:1806.09077*, 2018.
- J. Dean, G. Corrado, R. Monga, K. Chen, M. Devin, M. Mao, M. Ranzato, A. Senior, P. Tucker, K. Yang, et al. Large scale distributed deep networks. In *Advances in neural information processing systems*, pages 1223–1231, 2012.
- W. E. A proposal on machine learning via dynamical systems. *Communications in Mathematics and Statistics*, 5(1):1–11, 2017.
- S. Günther, L. Ruthotto, J. B. Schroder, E. C. Cyr, and N. R. Gauger. Layer-parallel training of deep residual neural networks. *SIAM Journal on Mathematics of Data Science*, 2(1):1–23, 2020.
- A. Gholami, K. Keutzer, and G. Biros. Anode: Unconditionally accurate memory-efficient gradients for neural odes. *arXiv preprint arXiv:1902.10298*, 2019.
- A. Gotmare, V. Thomas, J. Brea, and M. Jaggi. Decoupling backpropagation using constrained optimization methods. 2018.
- J. L. Gustafson. Reevaluating amdahl’s law. *Communications of the ACM*, 31(5):532–533, 1988.
- E. Haber, L. Ruthotto, E. Holtham, and S.-H. Jun. Learning across scales—multiscale methods for convolution neural networks. In *Thirty-Second AAAI Conference on Artificial Intelligence*, 2018.
- A. Harlap, D. Narayanan, A. Phanishayee, V. Seshadri, N. Devanur, G. Ganger, and P. Gibbons. Pipedream: Fast and efficient pipeline parallel dnn training. *arXiv preprint arXiv:1806.03377*, 2018.
- K. He, X. Zhang, S. Ren, and J. Sun. Deep residual learning for image recognition. In *Proceedings of the IEEE conference on computer vision and pattern recognition*, pages 770–778, 2016a.
- K. He, X. Zhang, S. Ren, and J. Sun. Identity mappings in deep residual networks. In *European Conference on Computer Vision*, pages 630–645. Springer, 2016b.
- R. Hecht-Nielsen. Theory of the backpropagation neural network. In *Neural networks for perception*, pages 65–93. Elsevier, 1992.
- Z. Huo, B. Gu, Q. Yang, and H. Huang. Decoupled parallel backpropagation with convergence guarantee. *arXiv preprint arXiv:1804.10574*, 2018.
- F. N. Iandola, M. W. Moskewicz, K. Ashraf, and K. Keutzer. Firecaffe: near-linear acceleration of deep neural network training on compute clusters. In *Proceedings of the IEEE Conference on Computer Vision and Pattern Recognition*, pages 2592–2600, 2016.
- M. Jaderberg, W. M. Czarnecki, S. Osindero, O. Vinyals, A. Graves, D. Silver, and K. Kavukcuoglu. Decoupled neural interfaces using synthetic gradients. In *Proceedings of the 34th International Conference on Machine Learning—Volume 70*, pages 1627–1635. JMLR. org, 2017.
- D. P. Kingma and M. Welling. Auto-encoding variational bayes. *arXiv preprint arXiv:1312.6114*, 2013.
- A. Kirby, S. Samsi, M. Jones, A. Reuther, J. Kepner, and V. Gadepally. Layer-parallel training with gpu concurrency of deep residual neural networks via nonlinear multigrid. In *2020 IEEE High Performance Extreme Computing Conference (HPEC)*, pages 1–7. IEEE, 2020.
- Y. LeCun, Y. Bengio, and G. Hinton. Deep learning. *nature*, 521(7553):436–444, 2015.
- J. Li, M. Xiao, C. Fang, Y. Dai, C. Xu, and Z. Lin. Training neural networks by lifted proximal operator machines. *IEEE Transactions on Pattern Analysis and Machine Intelligence*, 2020.
- Q. Li, L. Chen, C. Tai, and E. Weinan. Maximum principle based algorithms for deep learning. *The Journal of Machine Learning Research*, 18(1):5998–6026, 2017.
- D. Liberzon. *Calculus of variations and optimal control theory: a concise introduction*. Princeton University Press, 2011.
- Y. Lu, A. Zhong, Q. Li, and B. Dong. Beyond finite layer neural networks: Bridging deep architectures and numerical differential equations. *arXiv preprint arXiv:1710.10121*, 2017.
- Y. Maday and G. Turinici. A parareal in time procedure for the control of partial differential equations. *Comptes Rendus Mathématique*, 335(4):387–392, 2002.

- G. Marra, M. Tiezzi, S. Melacci, A. Betti, M. Maggini, and M. Gori. Local propagation in constraint-based neural network. *arXiv preprint arXiv:2002.07720*, 2020.
- T. Miyato, D. Okanohara, S.-i. Maeda, and M. Koyama. Synthetic gradient methods with virtual forward-backward networks. 2017.
- J. Nocedal and S. Wright. *Numerical optimization*. Springer Science & Business Media, 2006.
- T. Paine, H. Jin, J. Yang, Z. Lin, and T. Huang. Gpu asynchronous stochastic gradient descent to speed up neural network training. *arXiv preprint arXiv:1312.6186*, 2013.
- P. Parpas and C. Muir. Predict globally, correct locally: Parallel-in-time optimal control of neural networks. *arXiv preprint arXiv:1902.02542*, 2019.
- D. E. Rumelhart, G. E. Hinton, and R. J. Williams. Learning internal representations by error propagation. Technical report, California Univ San Diego La Jolla Inst for Cognitive Science, 1985.
- M. A. Tanner and W. H. Wong. The calculation of posterior distributions by data augmentation. *Journal of the American statistical Association*, 82(398):528–540, 1987.
- G. Taylor, R. Burmeister, Z. Xu, B. Singh, A. Patel, and T. Goldstein. Training neural networks without gradients: A scalable admm approach. In *International conference on machine learning*, pages 2722–2731, 2016.
- M. Thorpe and Y. van Gennip. Deep limits of residual neural networks. *arXiv preprint arXiv:1810.11741*, 2018.
- F. Tröltzsch. *Optimal control of partial differential equations: theory, methods, and applications*, volume 112. American Mathematical Soc., 2010.
- J. Zeng, S. Ouyang, T. T.-K. Lau, S. Lin, and Y. Yao. Global convergence in deep learning with variable splitting via the kurdyka-łojasiewicz property. *arXiv preprint arXiv:1803.00225*, 2018.
- J. Zeng, S.-B. Lin, and Y. Yao. A convergence analysis of nonlinearly constrained admm in deep learning. *arXiv preprint arXiv:1902.02060*, 2019.

## Supplementary Material

### A. Layer-Serial Training of Residual Networks

Without loss of generality, we consider the benchmark residual learning framework (He et al., 2016a;b) that assigns pixels in the raw input image to categories of interest as depicted in Figure 7. Its continuous-time analogue (Thorpe and van Gennip, 2018; E, 2017) is then introduced to bridge such an image classification task with a terminal control problem constrained by the so-called neural ordinary differential equation (Chen et al., 2018).

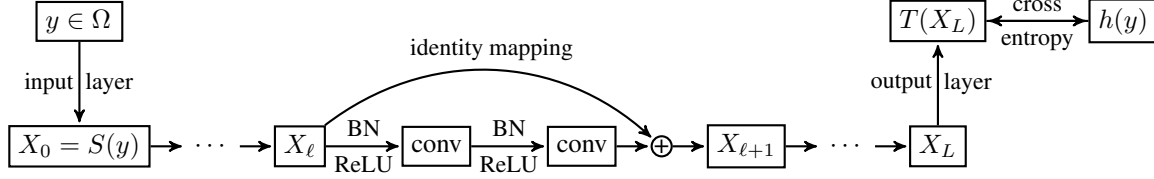


Figure 7. A diagram describing the serial training process of a pre-activation ResNet.

Given a human-labeled database  $\{y, h(y)\}_{y \in \Omega}$ , the optimization of network parameters requires solving problem (1), *i.e.*,

$$\arg \min_{\{W_\ell\}_{\ell=0}^{L-1}} \left\{ \mathbb{E}_{y \in \Omega} \left[ \|T(X_L) - h(y)\| \right] \mid X_0 = S(y), X_{\ell+1} = X_\ell + F(X_\ell, W_\ell) \text{ for } 0 \leq \ell \leq L-1 \right\}$$

where  $X_\ell$  indicates the input feature map of the  $\ell$ -th building module,  $L \in \mathbb{N}_+$  the total number of modules,  $F$  typically a composition of linear and nonlinear functions as depicted in Figure 7,  $W_\ell$  the network parameters to be learned, and  $\|\cdot\|$  a given metric measuring the discrepancy between the model prediction  $T(X_L)$  and the ground-truth label  $h(y)$  for each training sample  $y \in \Omega$ . The trainable parameters of input and output layers, *i.e.*,  $S$  and  $T$  in Figure 7, are assumed to be fixed (Haber et al., 2018) for the ease of illustration.

When the most commonly used backpropagation algorithm (Hecht-Nielsen, 1992) is applied to solving the optimization problem (1), we obtain formula (3) for parameter updates, *i.e.*,

$$W_\ell \leftarrow W_\ell - \eta \frac{\partial \varphi(X_L)}{\partial W_\ell} = W_\ell - \eta \frac{\partial \varphi(X_L)}{\partial X_{\ell+1}} \frac{\partial X_{\ell+1}}{\partial W_\ell}, \quad 0 \leq \ell \leq L-1,$$

where  $\eta > 0$  is the learning rate and  $\varphi(X_L) = \mathbb{E}_{y \in \Omega} [\|T(X_L) - h(y)\|]$ <sup>1</sup>.

Note that by defining  $P_{\ell+1} = \frac{\partial \varphi(X_L)}{\partial X_{\ell+1}}$  for  $0 \leq \ell \leq L-1$ , formula (3) can be rewritten as

$$W_\ell \leftarrow W_\ell - \eta \left( P_{\ell+1} \frac{\partial F(X_\ell, W_\ell)}{\partial W} \right), \quad 0 \leq \ell \leq L-1, \quad (12)$$

where  $\{P_{\ell+1}\}_{\ell=0}^{L-1}$  satisfy a backward dynamic that captures the objective changes with respect to hidden neurons, *i.e.*,

$$P_\ell = P_{\ell+1} \frac{\partial X_{\ell+1}}{\partial X_\ell} = P_{\ell+1} + P_{\ell+1} \frac{\partial F(X_\ell, W_\ell)}{\partial X}, \quad P_L = \frac{\partial \varphi(X_L)}{\partial X_L}. \quad (13)$$

To put it differently, the full serial backpropagation algorithm (3) is handled by formulae (13) and (12). Therefore, the training of ResNets at each iteration step requires the repeated execution of

- forward pass in (1)
- backward gradient propagation (13)
- parameter updates (12)

which can be very time-consuming as it is common to see neural networks with hundreds or even thousands of layers.

<sup>1</sup>Though the population risk is of primary interest, we only have access to the empirical risk in practice. For notational simplicity, we still denote by  $\varphi(\cdot)$  the objective function obtained from a mini-batch of the entire training data throughout this work.

### A.1. Optimal Control of Neural Ordinary Differential Equations

The continuous-time counterpart of the minimization problem (1) is formulated as (2), that is,

$$\arg \min_{\omega_t} \left\{ \mathbb{E}_{y \in \Omega} \left[ \|T(x_1) - h(y)\| \right] \mid x_0 = S(y), dx_t = f(x_t, w_t) dt \text{ for } 0 < t \leq 1 \right\}$$

where the forward propagation through the underlying network with fixed parameters, *i.e.*, the constraint of (1) is interpreted as a numerical discretization of differential equations (E, 2017; Lu et al., 2017; Chen et al., 2018).

By introducing the Lagrange functional with multiplier  $p_t$  (Nocedal and Wright, 2006), solving the constrained optimization problem (2) is equivalent to finding saddle points of the following Lagrange functional without constraints<sup>2</sup>

$$\begin{aligned} \mathcal{L}(x_t, w_t, p_t) &= \varphi(x_1) + \int_0^1 p_t (f(x_t, w_t) - \dot{x}_t) dt \\ &= \varphi(x_1) - p_1 x_1 + p_0 x_0 + \int_0^1 p_t f(x_t, w_t) + \dot{p}_t x_t dt. \end{aligned}$$

and the variation in  $\mathcal{L}(x_t, w_t, p_t)$  corresponding to a variation  $\delta w$  in control  $w$  takes on the form (Liberzon, 2011)

$$\delta \mathcal{L} = \left[ \frac{\partial \varphi(x_1)}{\partial x} - p_1 \right] \delta x + \int_0^1 \left( p_t \frac{\partial f(x_t, w_t)}{\partial x} + \dot{p}_t \right) \delta x + \left( p_t \frac{\partial f(x_t, w_t)}{\partial w} \right) \delta w dt,$$

which leads to the necessary conditions for  $w_t = w_t^*$  to be the extremal of  $\mathcal{L}(x_t, w_t, p_t)$ , *i.e.*,

$$\begin{aligned} dx_t^* &= f(x_t^*, w_t^*) dt, & x_0^* &= S(y), & \text{(state equation)} \\ dp_t^* &= -p_t^* \frac{\partial f(x_t^*, w_t^*)}{\partial x} dt, & p_1^* &= \frac{\partial \varphi(x_1^*)}{\partial x}, & \text{(adjoint equation)} \\ p_t^* \frac{\partial f(x_t^*, w_t^*)}{\partial w} &= 0, & 0 &\leq t \leq 1. & \text{(optimality condition)} \end{aligned}$$

However, directly solving this optimality system is computationally infeasible due to the so-called curse of dimensionality, a gradient-based iterative approach with step size  $\eta > 0$  is typically used, *e.g.*,

$$dx_t = f(x_t, w_t) dt, \quad x_0 = S(y), \quad \text{(forward pass)} \quad (15a)$$

$$dp_t = -p_t \frac{\partial f(x_t, w_t)}{\partial x} dt, \quad p_1 = \frac{\partial \varphi(x_1)}{\partial x}, \quad \text{(backward gradient propagation)} \quad (15b)$$

$$w_t \leftarrow w_t - \eta \left( p_t \frac{\partial f(x_t, w_t)}{\partial w} \right), \quad 0 \leq t \leq 1, \quad \text{(parameter updates)} \quad (15c)$$

which is consistent with the layer-serial training of ResNet through forward-backward propagation, *i.e.*, (1), (13) and (12), by taking the limit as  $L \rightarrow \infty$  (Li et al., 2017). In other words, the backpropagation approach (3) can be recovered from (4) and (5) by employing the stable discretization schemes (13) and (12).

## B. Augmented Lagrangian Method

Recall that the neural ODE-constrained optimization problem (2) can be reformulated as (7), that is,

$$\arg \min_{\{w_t^k\}_{k=0}^{K-1}} \left\{ \varphi(x_{s_K}^{K-1}) \mid x_{s_k}^{k-1} = \lambda_k \text{ and } x_{s_k}^k = \lambda_k, dx_t^k = f(x_t^k, w_t^k) dt \text{ on } (s_k, s_{k+1}] \text{ for } 0 \leq k \leq K-1 \right\},$$

whose the augmented Lagrangian functional is expressed as

$$\begin{aligned} \mathcal{L}_{\text{AL}}(x_t^k, p_t^k, w_t^k, \lambda_k, \kappa_k) &= \varphi(x_{s_K}^{K-1}) + \sum_{k=0}^{K-1} \left( \beta \psi(\lambda_k, x_{s_k}^{k-1}) - \kappa_k (\lambda_k - x_{s_k}^{k-1}) + \int_{s_k}^{s_{k+1}} p_t^k (f(x_t^k, w_t^k) - \dot{x}_t^k) dt \right) \\ &= \varphi(x_{s_K}^{K-1}) + \sum_{k=0}^{K-1} \left( \beta \psi(\lambda_k, x_{s_k}^{k-1}) - \kappa_k (\lambda_k - x_{s_k}^{k-1}) - p_{s_{k+1}}^k x_{s_{k+1}}^k + p_{s_k}^k \lambda_k + \int_{s_k}^{s_{k+1}} p_t^k f(x_t^k, w_t^k) + \dot{p}_t^k x_t^k dt \right). \end{aligned}$$

---

<sup>2</sup>For notational simplicity,  $\frac{dx_t}{dt}$  and  $\dot{x}_t$  are used to denote the time derivative of  $x_t$  throughout this work.

Specifically, the augmented Lagrangian functional can be decomposed as parts involving  $x_t^{K-1}$  and  $\{x_t^k\}_{k=0}^{K-2}$ , *i.e.*,

$$I = \varphi(x_{s_K}^{K-1}) - p_{s_K}^{K-1} x_{s_K}^{K-1} + p_{s_{K-1}}^{K-1} \lambda_{K-1} + \int_{s_{K-1}}^{s_K} p_t^{K-1} f(x_t^{K-1}, w_t^{K-1}) + \dot{p}_t^{K-1} x_t^{K-1} dt,$$

and

$$II = \sum_{k=0}^{K-2} \left( \beta \psi(\lambda_{k+1}, x_{s_{k+1}}^k) + (\kappa_{k+1} - p_{s_{k+1}}^k) x_{s_{k+1}}^k + p_{s_k}^k \lambda_k + \int_{s_k}^{s_{k+1}} p_t^k f(x_t^k, w_t^k) + \dot{p}_t^k x_t^k dt - \kappa_{k+1} \lambda_{k+1} \right)$$

respectively, then the variation in  $\mathcal{L}(x_t^k, p_t^k, w_t^k, \lambda_k, \kappa_k)$  corresponding to a variation  $\delta w_t^k$  in control  $w_t^k$  takes on the form

$$\begin{aligned} \delta \mathcal{L} = & \left( \frac{\partial \varphi(x_{s_K}^{K-1})}{\partial x} - p_{s_K}^{K-1} \right) \delta x^{K-1} + \int_{s_{K-1}}^{s_K} \left( p_t^{K-1} \frac{\partial f(x_t^{K-1}, w_t^{K-1})}{\partial x} + \dot{p}_t^{K-1} \right) \delta x^{K-1} dt \\ & + \sum_{k=0}^{K-2} \left[ \left( \beta \frac{\partial \psi(\lambda_{k+1}, x_{s_{k+1}}^k)}{\partial x} + \kappa_{k+1} - p_{s_{k+1}}^k \right) \delta x^k + \int_{s_k}^{s_{k+1}} \left( p_t^k \frac{\partial f(x_t^k, w_t^k)}{\partial x} + \dot{p}_t^k \right) \delta x^k dt \right], \end{aligned}$$

which implies that the adjoint variable  $p_t^k$  satisfies the backward differential equations (16) (Liberzon, 2011), namely,

$$\begin{aligned} dp_t^k &= -p_t^k \frac{\partial f(x_t^k, w_t^k)}{\partial x} dt \quad \text{on } [s_k, s_{k+1}), \\ p_{s_{k+1}}^k &= (1 - \delta) \left( \beta \frac{\partial \psi(\lambda_{k+1}, x_{s_{k+1}}^k)}{\partial x} + \kappa_{k+1} \right) + \delta \frac{\partial \varphi(x_{s_{k+1}}^k)}{\partial x}, \end{aligned} \quad (16)$$

for any  $0 \leq k \leq K-1$ . Here and in what follows  $\delta = \delta_{k, K-1}$  represents the Kronecker Delta function.

Moreover, it can be easily deduced from the augmented Lagrangian functional that the control updates satisfy

$$w_t^k \leftarrow w_t^k - \eta \left( p_t^k \frac{\partial f(x_t^k, w_t^k)}{\partial w} \right) \quad \text{on } [s_k, s_{k+1}] \quad (17)$$

for  $0 \leq k \leq K-1$ , while the correction of auxiliary variables takes on the form

$$\lambda_0 \equiv x_0 \quad \text{and} \quad \lambda_k \leftarrow \lambda_k - \eta \left( \beta \frac{\partial \psi(\lambda_k, x_{s_k}^{k-1})}{\partial \lambda} + p_{s_k}^k - \kappa_k \right) \quad \text{for } 1 \leq k \leq K-1. \quad (18)$$

Notably, by choosing a quadratic penalty function  $\psi(\lambda, x) = \|\lambda - x\|_{\ell_2}^2$ , formula (18) shows that the constraint violations associated with the minimizer of augmented Lagrangian method satisfy for  $1 \leq k \leq K-1$ ,

$$\lambda_k - x_{s_k}^{k-1} \approx \frac{1}{2\beta} (\kappa_k - p_{s_k}^k) \quad (19)$$

which offers two ways of improving the consistency constraint  $x_{s_k}^{k-1} = x_{s_k}^k$ : increasing  $\beta$  or sending  $\kappa_k \rightarrow p_{s_k}^k$ , whereas the penalty method (by forcing  $\kappa_k \equiv 0$  in (19), see also the formula (24) below) provides only one option. Moreover, it can be deduced from (19) that the update rule of explicit Lagrange multipliers satisfy

$$\kappa_0 \equiv 0 \quad \text{and} \quad \kappa_k \leftarrow \kappa_k - \frac{\eta}{2\beta} (\lambda_k - x_{s_k}^{k-1}) \quad \text{for } 1 \leq k \leq K-1. \quad (20)$$

In short, the augmented Lagrangian method for approximately solving problem (2) at each iteration step includes

- local operations (6), (16), (17) in parallel
- global communication (18), (20)

which not only parallelizes the iterative system (15) for solving (2) but also lessens the the issue of coefficient tuning.

### B.1. Penalty Method

Note that by forcing  $\kappa_k \equiv 0$  for any  $0 \leq k \leq K - 1$ , the augmented Lagrangian method degenerates to a penalty method. Specifically, it can be deduced from (16) that the adjoint equation for relaxed minimization problem (8) takes on the form

$$\begin{aligned} dp_t^k &= -p_t^k \frac{\partial f(x_t^k, w_t^k)}{\partial x} dt \quad \text{on } [s_k, s_{k+1}), \\ p_{s_{k+1}}^k &= (1 - \delta) \beta \frac{\partial \psi(\lambda_{k+1}, x_{s_{k+1}}^k)}{\partial x} + \delta \frac{\partial \varphi(x_{s_{k+1}}^k)}{\partial x}, \end{aligned} \quad (21)$$

for  $0 \leq k \leq K - 1$ . Moreover, by (17) and (18), the update rule for control variables now satisfies for  $0 \leq k \leq K - 1$ ,

$$w_t^k \leftarrow w_t^k - \eta \left( p_t^k \frac{\partial f(x_t^k, w_t^k)}{\partial w} \right) \quad \text{on } [s_k, s_{k+1}], \quad (22)$$

while the correction of auxiliary variables is given by

$$\lambda_0 \equiv x_0 \quad \text{and} \quad \lambda_k \leftarrow \lambda_k - \eta \left( \beta \frac{\partial \psi(\lambda_k, x_{s_k}^{k-1})}{\partial \lambda} + p_{s_k^+}^k \right) \quad \text{for } 1 \leq k \leq K - 1. \quad (23)$$

In short, the penalty approach (8) for approximately solving problem (2) at each iteration consists of

- local operations (6), (21), (22) in parallel
- global communication (23)

which parallelizes the iterative system (15) for solving (2).

In particular, by choosing the quadratic penalty function  $\psi(\lambda, x) = \|\lambda - x\|_{\ell_2}^2$  as before, it can be deduced from (23) that the constraint violations associated with the approximate minimizer of problem (8) satisfies for  $1 \leq k \leq K - 1$ ,

$$\lambda_k - x_{s_k}^{k-1} \approx -\frac{1}{2\beta} p_{s_k^+}^k \quad (24)$$

which implies that a large penalty coefficient  $\beta$  is needed in order to force the minimizer of (8) close to the feasible region of problem (2). By employing the augmented Lagrangian method (19), the ill-conditioning of penalty method can be lessened without increasing the penalty coefficient indefinitely, however, the introduction of external Lagrangian multipliers  $\{\kappa_k\}_{k=0}^{K-1}$  requires additional memory and communication overheads that may hamper the speed-up ratio.

## C. Parallel Backpropagation and Communication

By utilizing the consistent finite difference schemes (see Appendix A) for the discretization of the time-parallel iterative systems established in subsection 2.2, we arrive at a layer-parallel training algorithm that enables us to fully leveraging the computing resources. The detailed derivations are presented in what follows.

Recall the partitioning of  $[0, 1]$  associated with the original ResNet (1), *i.e.*,

$$0 = t_0 < t_1 < \dots < t_\ell = \ell \Delta t < t_{\ell+1} < \dots < t_{L=nK} = 1,$$

then the local sub-problem is built by choosing a coarsening factor  $n > 1$  and extracting every  $n$ -th module as depicted in Figure 2, or, equivalently, the forward Euler discretization of neural ODE with the coarser grid introduced in subsection 2.2

$$t_0 = s_0 < \dots < s_k = t_{nk} < s_{k+1} < \dots < s_K = t_L,$$

which can be implemented independently and trained with low accuracy at a correspondingly low cost<sup>3</sup>.

<sup>3</sup>The trainable parameters in the input and output layers, *i.e.*,  $S$  and  $T$ , can be automatically updated by coupling into the first and last sub-problems respectively.

To be specific,  $[s_k, s_{k+1}]$  is uniformly divided into  $n$  sub-intervals for  $0 \leq k \leq K - 1$ , *i.e.*,

$$s_k = t_{kn} < t_{kn+1} < \dots < t_{kn+n-1} < t_{kn+n} = s_{k+1},$$

we have by (6) that feature flow of the  $k$ -th sub-network evolves according to

$$X_{kn}^k = \lambda_k, \quad X_{kn+m+1}^k = X_{kn+m}^k + F(X_{kn+m}^k, W_{kn+m}^k) \quad (25)$$

where  $0 \leq m \leq n - 1$ . Then by using the particular numerical scheme (13) that arises from the discrete-to-continuum transition in subsection 2.1, the discretization of the adjoint equation (16) is given by the backward dynamic

$$\begin{aligned} P_{kn+m}^k &= P_{kn+m+1}^k + P_{kn+m+1}^k \frac{\partial F(X_{kn+m}^k, W_{kn+m}^k)}{\partial X} = P_{kn+m+1}^k \frac{\partial X_{kn+m+1}^k}{\partial X_{kn+m}^k}, \\ P_{kn+n}^k &= (1 - \delta) \left( \beta \frac{\partial \psi(\lambda_{k+1}, X_{kn+n}^k)}{\partial X} + \kappa_{k+1} \right) + \delta \frac{\partial \varphi(X_{kn+n}^k)}{\partial X}. \end{aligned} \quad (26)$$

In other words, for any interval  $[s_k, s_{k+1}]$  and arbitrary  $0 \leq m \leq n$ , the adjoint variable in (26) is equivalent to

$$P_{kn+m}^k = (1 - \delta) \left( \beta \frac{\partial \psi(\lambda_{k+1}, X_{kn+n}^k)}{\partial X_{kn+m}^k} + \kappa_{k+1} \frac{\partial X_{kn+n}^k}{\partial X_{kn+m}^k} \right) + \delta \frac{\partial \varphi(X_{kn+n}^k)}{\partial X_{kn+m}^k} \quad (27)$$

which captures the objective and layer-wise synthetic loss changes, namely, the second and the first term on the right-hand-side of (27), with respect to the latent states for  $k = K - 1$  and  $0 \leq k \leq K - 2$ , respectively.

Contrary to the straightforward approach (Maday and Turinici, 2002; Günther et al., 2020) where the iterations are executed by first solving state equation (6), then adjoint equation (21) afterwards, and finally control updates (22), we conduct the control updates simultaneously with the solution of adjoint equation after solving the state equation.

Specifically, to discretize the update rule for control variables (17) for any  $0 \leq k \leq K - 1$ , *i.e.*,

$$w_t^k \leftarrow w_t^k - \eta \left( p_t^k \frac{\partial f(x_t^k, w_t^k)}{\partial w} \right) \quad \text{on } [s_k, s_{k+1}],$$

we adopt the numerical scheme (12) to guarantee the accurate gradient information (Gholami et al., 2019), that is,

$$\begin{aligned} W_{kn+m}^k &\leftarrow W_{kn+m}^k - \eta \left( P_{kn+m+1}^k \frac{\partial F(X_{kn+m}^k, W_{kn+m}^k)}{\partial W} \right) \\ &= W_{kn+m}^k - \eta \left( (1 - \delta) \left( \beta \frac{\partial \psi(\lambda_{k+1}, X_{kn+n}^k)}{\partial X_{kn+m+1}^k} + \kappa_{k+1} \frac{\partial X_{kn+n}^k}{\partial X_{kn+m+1}^k} \right) + \delta \frac{\partial \varphi(X_{kn+n}^k)}{\partial X_{kn+m+1}^k} \right) \frac{\partial X_{kn+m+1}^k}{\partial W_{kn+m}^k} \\ &= W_{kn+m}^k - \eta \left( (1 - \delta) \left( \beta \frac{\partial \psi(\lambda_{k+1}, X_{kn+n}^k)}{\partial W_{kn+m}^k} + \kappa_{k+1} \frac{\partial X_{kn+n}^k}{\partial W_{kn+m}^k} \right) + \delta \frac{\partial \varphi(X_{kn+n}^k)}{\partial W_{kn+m}^k} \right) \end{aligned} \quad (28)$$

where the second equality holds by (25) and (27). Next, we have by (18) and (27) that the correction of auxiliary variables satisfies  $\lambda_0 \equiv x_0$  and

$$\lambda_k \leftarrow \lambda_k - \eta \left( \beta \frac{\partial \psi(\lambda_k, X_{kn}^{k-1})}{\partial \lambda} + (1 - \delta) \left( \beta \frac{\partial \psi(\lambda_{k+1}, X_{kn+n}^k)}{\partial X_{kn}^k} + \kappa_{k+1} \frac{\partial X_{kn+n}^k}{\partial X_{kn}^k} \right) + \delta \frac{\partial \varphi(X_{kn+n}^k)}{\partial X_{kn}^k} - \kappa_k \right) \quad (29)$$

for  $1 \leq k \leq K - 1$ , while the update rule (20) for Lagrangian multiplier  $\kappa_k$  is given by

$$\kappa_0 = 0 \quad \text{and} \quad \kappa_k \leftarrow \kappa_k - \frac{\eta}{2\beta} (\lambda_k - X_{kn}^{k-1}) \quad (30)$$

for  $1 \leq k \leq K - 1$ . Clearly, operations (29) and (30) require communication between adjacent layers which can impede the performance of parallel computations.

Consequently, the layer-parallel training approach for solving (1) can be formulated as the sequential operations

- decoupled forward pass and backpropagation (25), (28)
- global communication (29), (30)

at each iteration, which breaks the forward, backward and update locking issues (Jaderberg et al., 2017).

## D. Initialization of Algorithm 1

**Algorithm 1:** Initialization of the Layer-parallel Training Algorithm

// Initialization.

- [1] divide the ResNet model into  $K$  local sub-models (e.g., the uniform decomposition depicted in Figure 2);
- [2] generate the initial guess of parameters and auxiliary variables (e.g., copy from a ResNet trained with one epoch);
- [3] use a proper metric (e.g., squared  $\ell_2$ -norm) and coefficients (e.g., an increasing sequence) for penalty function;
- [4] set Lagrangian multipliers to zero; // degenerate to penalty method if  $\kappa_k \equiv 0$  hereafter
- [5] schedule proper learning rates for network parameters  $\eta_w$ , auxiliary variables  $\eta_\lambda$ , and multipliers  $\eta_\kappa$ ;

## E. Additional Experiments

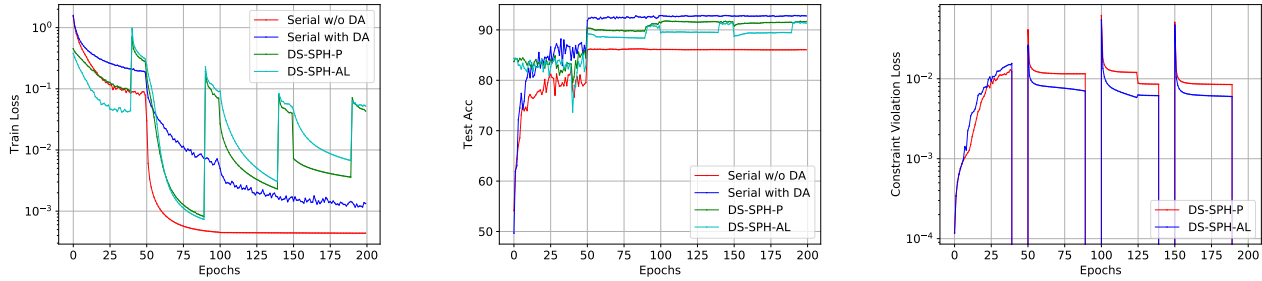


Figure 8. Training loss through the full serial forward pass, testing loss and constraint violation for ResNet-110 on CIFAR-10 dataset, where  $K = 3$  and  $\gamma_H = 1/4$  (the serial and parallel portions are executed alternatively).

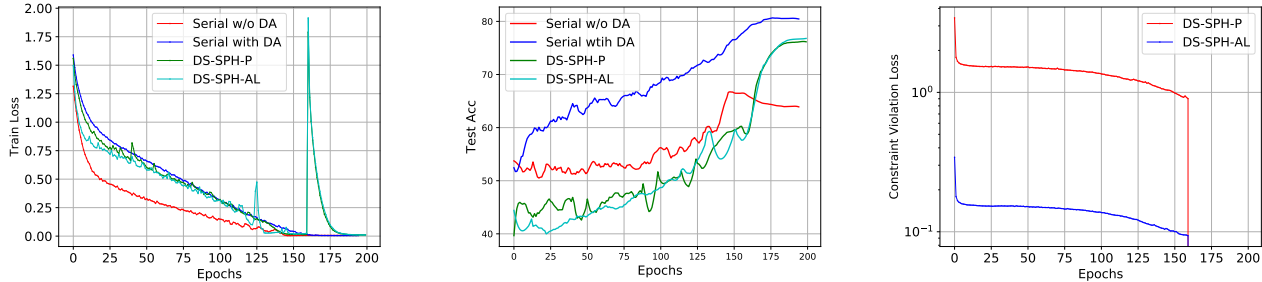


Figure 9. Training loss through the full serial forward pass, testing loss and constraint violation for WideResNet on CIFAR-100 dataset, where  $K = 3$  and  $\gamma_H = 1/4$  (the parallel portion is first executed, followed by the serial portion to finish the training).

**Learning curves.** We show in Figure 8 and Figure 9 the learning curves of ResNet on CIFAR-10 and WideResNet on CIFAR-100, respectively. As can be seen from Figure 8 (right) and Figure 9 (right), a large jump of constraint violation appears when the training is switched from parallel to serial, which helps improve the network parameters together with the use of data augmentation (see Figure 8 (left and middle) and Figure 9 (left and middle)). Moreover, by using the same penalty coefficient, the constraint violation associated with AL method is smaller than that of penalty method (see Figure 8 (right) and Figure 9(right)), which validates our theoretical analysis (24) and (19).